Effect of surfactant on bubble collisions on a free surface

Shiyan Wang,[1] Tianqi Guo,[1] Sadegh Dabiri,[1,2] Pavlos P. Vlachos,[1] and Arezoo M. Ardekani[1,*]
[1]*School of Mechanical Engineering, Purdue University, West Lafayette, Indiana 47907, USA*
[2]*Department of Agricultural and Biological Engineering, Purdue University, West Lafayette, Indiana 47907, USA*
(Received 21 August 2016; published 18 April 2017)

We report on the coefficient of restitution of bubble collision on a free surface in the presence of surfactants. In pure fluids, the collision process is well described by a competition between thin film drainage and interfacial tension. When surfactants are introduced in pure water, they generate Marangoni stresses on both the bubble interface and free surface, which provides an additional mechanism affecting the collision process. We investigate this mechanism for the bubble collision process in surfactant solutions through a combination of experimental and numerical approaches, with results showing a reduced rebound velocity during the collision process in surfactant solutions compared with that in pure water. Furthermore, by varying both bubble size and surfactant concentration, our experiments show that bubbles experience elastic, partially inelastic, and perfectly inelastic collisions. We identify the Langmuir number, the ratio between absorption and desorption rates, as the fundamental parameter that quantifies the Marangoni effect on the collision process. The effect of Marangoni stress on the bubble's coefficient of restitution is nonmonotonic, where the coefficient of restitution first decreases with Langmuir number and then increases.

DOI: 10.1103/PhysRevFluids.2.043601

I. INTRODUCTION

Surfactants are known to effectively reduce the rate at which bubbles rise in pure fluids [1,2]. The first physical explanation of this phenomenon was given by Frumkin and Levich [3]. For a translating bubble, surfactants on the bubble interface are adsorbed from the bulk solution, generating Marangoni stresses that reduce interfacial mobility and increase the drag acting on the rising bubble. To date, several papers have discussed the effect of surfactants on a bubble's drag coefficient [4,5], its lift force under shear flow [6], and its steady-state velocity [1,7]. For a bubble rising rectilinearly in a surfactant solution, the reduced steady-state velocity can be simulated using a stagnant cap model, which assumes a no-slip velocity within the cap region and zero shear condition at the remaining portion of the bubble interface [1]. Cuenot *et al.* [4] solved the full Navier-Stokes equations coupled with the bulk and interfacial surfactant concentration equations. Their numerical study confirmed the validity of the stagnant-cap model, and furthermore, they studied the transient evolution of the flow over a spherical bubble in surfactant solutions.

Large bubbles [8] and multiple bubble interactions [2] have been observed in practical systems, where the effects of nonspherical shape and dynamic interfacial interactions need to be considered. For an isolated large air bubble (diameter larger than 2 mm) in quiescent water, surfactants change its path instability [8]. Recent numerical simulations [9–11] have revealed the significance of a surfactant affecting the transient behavior of a nonspherical bubble. In a bubbly flow, surfactants could change the flow structure by altering bubble-bubble interactions and inhibiting the coalescence of small bubbles [2].

Studies on interactions between air bubbles and the free surface are important for both environmental and industrial applications. The interactions may lead to the coalescence of gas

*ardekani@purdue.edu

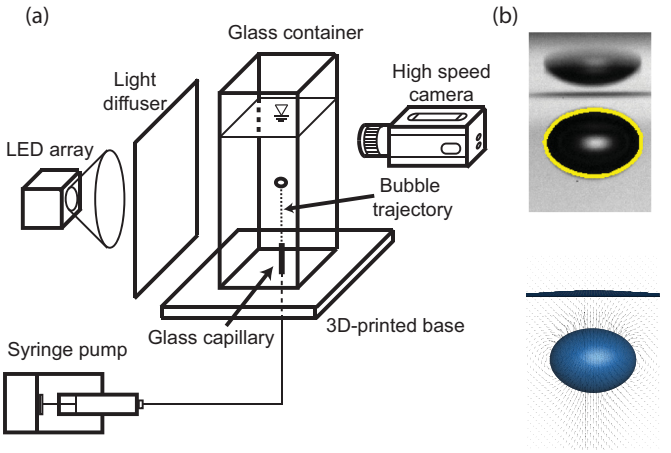

FIG. 1. (a) The schematic diagram of the experimental setup. (b) A direct comparison of a raw image of an ascending bubble ($R = 0.66$ mm) using experiments and 3D numerical simulation in pure water. The vectors in the 3D numerical simulation indicate flow velocity.

bubbles in mass transfer equipment such as bubble columns, decreasing overall interfacial area [12]. Despite decades of research studying the collision process in pure liquids [13–17], the relevant bubble dynamics in surfactant solutions are poorly understood. In this work, we conduct experimental studies, aided by the numerical simulations, to examine the effect of a surfactant on rising bubbles colliding on a free surface. Section II describes the experimental setup. We report the mathematical models and numerical implementations for multiphase flows in surfactant solutions in Sec. III. In Sec. IV, we first compare the bubble dynamics in both pure water and surfactant solutions. Subsequently, we examine the effect of surfactants on both the drag acting on the rising bubbles and their collision processes. Finally, we conclude with our findings of this study in Sec. V.

II. EXPERIMENTAL SECTION

The experimental setup is shown in Fig. 1(a). Air bubbles were generated by either a borosilicate glass capillary or a stainless-steel needle that was installed at the center of the three-dimensional (3D) printed base and was connected with a precision syringe pump (PHD Ultra) from Harvard Apparatus. Generated bubble radii ranged from 0.44 to 0.84 mm. The test container (size: 1 in. $\times$ 1 in. $\times$ 4 in.) was made of borosilicate glass. Before conducting each experiment, we eliminated the container's contaminations using an ultrasonic bath with ultrapure water. The ultrapure water was supplied by a purification system (Barnstead MicroPure UF/UV, Thermo Scientific). Its electric resistivity was 18.2 MΩ cm (18.18 MΩ cm for ultrapure water [18]). The conductivity and total organic carbon in the water were 0.055 μS cm^{-1} and 5 ppb, respectively. We chose 1-pentanol as our surfactant model due to its well-known kinematics of dynamic adsorption [19,20]. The concentration of the 1-pentanol solution ranged from 0 to 200 mM [0% to 8% of critical micellar concentration (CMC)]. The surface tension value between the air and 1-pentanol solution was measured using a pendant droplet tensiometer (Ramé-Hart 500) and was found to be in good agreement with the Szyszkowski equation [21] (see Appendix A). A complementary metal-oxide semiconductor (CMOS) camera (Phantom Miro M340, Vision Research) mounted on a microstage recorded images at 1600–3000 frames/s. The images were preprocessed by taking the inverse intensity and a subsequent local minimum background subtraction to eliminate background noise. The bubble center was determined by calculating the geometric center of the generated binary image with a preselected intensity threshold. The instantaneous bubble velocity was obtained by taking the central difference of the bubble's vertical position with respect to time. The temporal evolution of the translational velocity

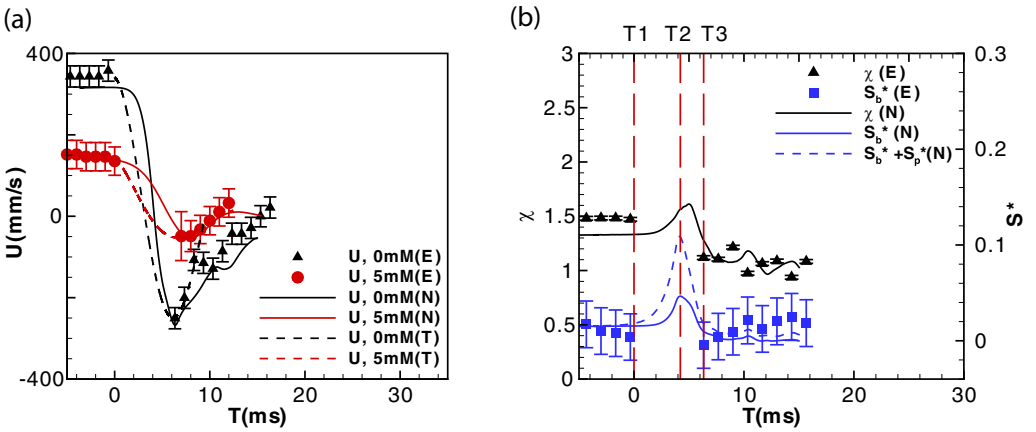

FIG. 2. (a) The bubble's vertical velocity during the collision process for 0 and 5 mM 1-pentanol solutions obtained using (E) experimental, (N) numerical, and (T) theoretical studies. (b) In pure water, the temporal evolution of the bubble's deformation χ and dimensionless surface change S^* are recorded through numerical simulations and experiments. Error bars indicate the uncertainty of experimental measurements (see Appendix B). The bubble's size is $R = (6\mathcal{V}_b/\pi)^{1/3}/2 = 0.66$ mm, where $\mathcal{V}_b$ is the bubble volume. In the theoretical model, the collision process is modeled as an underdamped mass-spring system (see Appendix C).

of a 0.66-mm bubble in both pure water (black solid triangles) and a 5 mM 1-pentanol solution (red solid circles) is shown in Fig. 2(a). We should note that there is a period during which the bubble collides on and is in contact with the free surface, and position and centroid measurements contain large error. Consequently, measurement uncertainties for the bubble centroid are large. Therefore, we exclude all experimental data for this period in Fig. 2.

III. MATHEMATICAL MODEL AND NUMERICAL IMPLEMENTATION

A. Mathematical model

In this section, we describe the mathematical model for both the rising motion of gas bubbles and their collisions on a free surface [see Fig. 1(b)]. Both gas and liquid phases are homogenous fluids. The equations of motion for viscous, incompressible fluids in the entire computational domain are

$$\nabla \cdot \mathbf{u} = 0, \tag{1}$$

$$\rho \frac{D\mathbf{u}}{Dt} = -\nabla p + \mu \nabla^2 \mathbf{u} + \rho \mathbf{g} + \mathbf{f}, \tag{2}$$

where t is time, $\mathbf{u}$ is the flow velocity, p is the hydrodynamic pressure, $\mathbf{g}$ is the gravitational acceleration, μ is the dynamic viscosity of the fluid, and ρ is the fluid density. $D(\cdot)/Dt$ is the material derivative. Since fluid properties remain constant within each phase, $\frac{D\rho}{Dt} = 0$ and $\frac{D\mu}{Dt} = 0$. The density ρ and viscosity μ can be written as $\rho = \rho_i + \phi(\rho_o - \rho_i)$ and $\mu = \mu_i + \phi(\mu_o - \mu_i)$, where subscripts i and o refer to gas phase and liquid phase, respectively; the indicator function ϕ separates two phases, with $\phi = 1$ for the bulk liquid and $\phi = 0$ for the gas phase. The surface tension force $\mathbf{f}$ in the momentum equation, Eq. (2), acts on the interfaces (free surface and bubble interface),

$$\mathbf{f} = 2\int_A \sigma\kappa\mathbf{n}\delta(\mathbf{x} - \mathbf{x}_f)dA, \tag{3}$$

where σ is the surface tension coefficient, dA is the surface differential element, κ is the mean curvature of the interface, and $\mathbf{n}$ is the unit vector normal to the interface. The interface can be

TABLE I. Parameters for the 5 mM 1-pentanol solution.

Parameter	Value
Temperature (°C)	2.1×10^{1}
Surface tension of pure water (dyn/cm)	7.2×10^{1}
Surface tension of 5 mM 1-pentanol (dyn/cm)	6.8×10^{1}
Maximum interfacial surfactant concentration Γ_∞ (mol/cm^2)	5.9×10^{-10}
Adsorption kinematic coefficient k_a (cm/s)	3.0×10^{-3}
Desorption kinematic coefficient k_d (s^{-1})	1.1×10^{2}
Bubble size R (mm)	6.6×10^{-1}

described by a collection of distributed points $\mathbf{x}_f$. The three-dimensional delta function δ is used to calculate interfacial force, which is nonzero only on the interface.

Surfactants are soluble, and mass transfer occurs between the bulk fluid and the interface. We write the convection-diffusion equations for both bulk concentration C and interfacial concentration Γ, respectively,

$$\frac{\partial C}{\partial t} + \nabla \cdot (\mathbf{u}C) = \nabla \cdot (D_c \nabla C) + \dot{S}_c, \tag{4}$$

$$\frac{\partial \Gamma}{\partial t} + \nabla_s \cdot (\Gamma \mathbf{U}_s) = D_s \nabla_s^2 \Gamma + \dot{S}_\Gamma, \tag{5}$$

where $\mathbf{U}_s$ is the tangential velocity on the interface. The surfactant is impermeable to the gas phase; therefore, $D_c = D_o\phi$, where D_o is the molecular diffusion coefficient of the surfactant in the bulk liquid. $\nabla_s = \nabla - \mathbf{n}(\mathbf{n} \cdot \nabla)$ is the surface gradient defined at the interface; D_s is the interfacial diffusion coefficient of the surfactant. The dynamic adsorption of the surfactant on the interface is given by

$$\dot{S}_\Gamma = k_a C_s (1 - \Gamma/\Gamma_\infty) - k_d \Gamma, \tag{6}$$

and this source term is related to the bulk concentration via the following relationship:

$$\dot{S}_\Gamma = -D_c (\mathbf{n} \cdot \nabla C|_{C=C_s}), \tag{7}$$

where k_a and k_d are the adsorption and desorption rate constants, respectively; C_s is the surfactant bulk concentration evaluated adjacent to the interface; and Γ_∞ is the maximum interfacial surfactant concentration. The value of the surface tension coefficient is directly affected by the interfacial surfactant concentration Γ, and it is written as $\sigma/\sigma_0 = 1 + \beta \ln(1 - \Gamma/\Gamma_\infty)$, where $\beta = \mathscr{R}T\Gamma_\infty/\sigma_0$ characterizes the sensitivity of the surface tension σ to the interfacial surfactant concentration Γ, $\mathscr{R}$ is the ideal gas constant, and σ_0 is the surface tension of a clean interface at room temperature T. For our experiments, the room temperature is kept at 21°C, and σ_0 is about 72.2 mN/m, which is consistent with previous literature [19,20]. Therefore, for the 1-pentanol solution, $\beta = 0.20$. The time scale [8] for achieving the equilibrium interfacial surfactant concentration can be estimated as $\tau_e \sim (k_a C_\infty/\Gamma_\infty + k_d)^{-1}$, where C_∞ is the initial surfactant bulk concentration. Therefore, a surfactant solution with a high bulk concentration quickly reaches equilibrium. For the 1-pentanol solution, Γ_∞, k_a, and k_d are invariant under different bulk concentrations [19,20]: $\Gamma_\infty = 5.90 \times 10^{-10}$ mol cm^{-2}, $k_a = 3.00 \times 10^{-3}$ cm s^{-1}, and $k_d = 1.10 \times 10^{2}$ s^{-1}. For a 0.66-mm-radius bubble in a 1 mM 1-pentanol solution, the dimensionless distance x_e/R for reaching the equilibrium state can be estimated as $x_e/R \sim \rho g R \tau_e/(9\mu) = 6.25$. In both experiments and numerical simulations, domain sizes are large enough that the interfacial surfactant concentration reaches the equilibrium state, and the bubble reaches steady-state velocity U_t before colliding on the free surface. Parameters corresponding to a 5 mM 1-pentanol solution are listed in Table I.

TABLE II. Dimensionless parameters for a 5 mM 1-pentanol solution.

Parameter	Value
Reynolds number, $\mathrm{Re}_U = 2\rho U R/\mu$	6.3×10^2
Capillary number, $\mathrm{Ca}_U = \mu U/\sigma$	6.6×10^{-3}
Bulk Péclet number, $\mathrm{Pe} = 2UR/D_c$	6.3×10^1
Interfacial Péclet number, $\mathrm{Pe}_S = 2UR/D_S$	6.3×10^1
Density ratio, ρ_i/ρ_o	8.2×10^2
Viscosity ratio, μ_i/μ_o	5.5×10^2
Adsorption kinematics, $k = k_a C_\infty/k_d\Gamma_\infty$	2.3×10^{-1}
Biot number, $\mathrm{Bi} = 2k_d R/U$	3.1×10^{-1}
Damkohler number, $\mathrm{Da} = \Gamma_\infty/2RC_\infty$	8.9×10^{-4}
Elasticity number, $\beta_S = RT\Gamma_\infty/\sigma$	2.0×10^{-1}

The list of dimensionless parameters is summarized in Table II. The characteristic velocity of the bubble $U = \rho g R^2/9\mu$ is used to evaluate dimensionless parameters. Note that there is no fitting parameter in the numerical simulations.

B. Numerical implementation

A front-tracking and finite-volume method [22,23] is applied to solve Eqs. (2) and (4) on fixed uniform Cartesian staggered grids. The time discretization is obtained using the first-order Euler method. Diffusion terms in Eqs. (2) and (4) are solved using central-difference schemes. In Eqs. (2) and (4), the convection terms are solved using a quadratic upstream interpolation for convective kinetics (QUICK) [24] and a fifth-order weighted essentially nonoscillatory (WENO-Z) scheme [25], respectively. The projection method is utilized to enforce the continuity condition in Eq. (1), and the resultant Poisson equation for the pressure is solved using the HYPRE library [26]. Both the bubble interface and free surface are represented by unstructured Lagrangian triangular grids. Equation (5), which governs the evolution of interfacial surfactant concentration, is solved on these Lagrangian grids. On each triangular element Δ_e, Eq. (5) is written in an integral form,

$$\frac{d}{dt}\int_{\Delta_e}\Gamma dA = D_s\int_{\Delta_e}\nabla_s^2\Gamma dA + \int_{\Delta_e}\dot{S}_\Gamma dA. \tag{8}$$

The term on the left hand side of Eq. (8) is solved using a first order explicit Euler method; the surface Laplacian term in Eq. (8) is solved in an identical way used for the calculation of curvature κ in Eq. (2). More details on the numerical implementation can be found in Refs. [11,22,23].

In the simulation, a spherical bubble of radius R is initially placed at the center of the x-y plane and rises from location z_o, which is $2R$ away from the bottom. The size of the computational domain is $9R \times 9R \times 36R$ in the x, y, and z directions, respectively. The free surface is located $3R$ away from the top of the computational domain. Flow field $\mathbf{u}$, pressure p, and surfactant bulk concentration C satisfy the periodic condition at side boundaries of the rectangular computational domain while both top and bottom boundaries satisfy no-slip wall boundary conditions.

IV. RESULTS AND DISCUSSION

A. Collision process in pure water and the 1-pentanol solution

In Fig. 2, experimental observations indicate that the presence of a surfactant significantly modifies the collision process compared with pure water (also see Movie 1 in the Supplemental Material [27]). Here we focus on the first collision of a 0.66-mm bubble with the free surface. In order to characterize the collision process, three distinct time instants are identified in Fig. 2(b). T1, T2, and T3 correspond

to the instants when the free surface starts affecting the bubble velocity ($U|_{\mathrm{T=T1}} = 0.95U_t$), when the bubble velocity becomes zero after colliding on the free surface, and when the bubble reaches a maximum velocity after reversing its direction of motion, respectively. Therefore, the precollision stage is defined as the period of time from T1 to T2, and the postcollision stage is from T2 to T3.

A comparison of total energy transfer during the collision between pure water and the surfactant solution can facilitate the interpretation of the collision dynamics. We compare the total energy transfer of the collision process. The instantaneous total energy consists of surface energy due to the deformation of the bubble, surface energy due to the deformation of the free surface, and kinetic energy associated with the translation of the bubble. At time T1, the normalized total energy E^*_{T1} is written as

$$E^*_{\mathrm{T1}} = \frac{\Delta E|_{\mathrm{T=T1}}}{E_r} = \left(\frac{E_k}{E_r} + S^*_b + S^*_p\right)\Big|_{\mathrm{T=T1}}, \tag{9}$$

where $\Delta E = E - E_r$, E is the total energy of the bubble and free surface, $E_r = 4\pi\sigma R^2$ is the energy of a spherical bubble with the equivalent radius R at rest [13], $E_k = C_M(\chi)\rho\mathcal{V}_b U^2/2$ is the kinetic energy associated with the bubble motion, χ is the deformation of the bubble, and C_M is the added mass coefficient by assuming the bubble's shape to be an oblate spheroid [28,29],

$$C_M = \frac{(\chi^2-1)^{1/2} - \cos^{-1}\chi^{-1}}{\cos^{-1}\chi^{-1} - (\chi^2-1)^{1/2}\chi^{-2}}. \tag{10}$$

Changes in the surface area of the bubble interface and the free surface in dimensionless form are represented as $S^*_b = \Delta S_b/(4\pi R^2)$ and $S^*_p = \Delta S_p/(4\pi R^2)$, respectively. Even though the surface tension values for pure water and the surfactant solution are comparable (72.2 and 67.9 dyn/cm measured at $T = 21^\circ$C, respectively), the estimated energy E^*_{T1} for water is about 7.45 times larger than that in the 5 mM 1-pentanol solution. This is due to the large bubble velocity in pure water ($\mathrm{Re} = 2\rho U_t R/\mu = 438$) compared with that in the 5 mM 1-pentanol solution ($\mathrm{Re} = 195$), shown in Fig. 2(a). At time T2, $E^*_{\mathrm{T2}} = (S^*_b + S^*_p)|_{\mathrm{T=T2}}$. During the precollision stage, the bubble kinetic energy is transferred to the surface energy of both the bubble interface and free surface. The computation of $E^*_{\mathrm{T2}}/E^*_{\mathrm{T1}}$ is only available using the numerical simulations, and we find this ratio to be 88.7% for pure water and 74.4% for the 5 mM 1-pentanol solution. The second phase of the collision process corresponds to the postcollision stage. From Fig. 2, at time T3, the total surface change ($S^*_b + S^*_p$) is close to zero, and the kinetic energy associated with the bubble motion reaches its maximum.

During the entire bubble collision process, the total energy loss can be quantified by the coefficient of restitution, $\varepsilon = -U_{\mathrm{T3}}/U_{\mathrm{T1}}$. There is no energy loss when $\varepsilon = 1$. In the pure water experiment, the coefficient of restitution is 0.73. The large value of the coefficient of restitution ($\varepsilon \geqslant 0.7$) indicates an elastic collision. However, in the 5 mM 1-pentanol solution, we find this coefficient to be 0.32, and the bubble eventually detaches from the free surface. This reduced coefficient of restitution indicates a significant energy loss during the collision process, leading to a surfactant-induced partially inelastic collision.

The reduced rebound velocity in the surfactant solution can be explained by exploring the flow structure around a bubble in both pure water and the 5 mM 1-pentanol solution during the collision process (see Movie 2 [27]). At time T1, a thin wake structure is formed in pure water due to the slip condition at the bubble interface [Fig. 3(c)]. However, the bubble's wake in the 5 mM 1-pentanol solution [Fig. 3(b)] is distinct from that of a clean bubble. By visualizing the interfacial surfactant concentrations Γ on the bubble interface [see Fig. 3(b) at T1], we observe that surfactant molecules migrate toward the rear of the bubble, where Γ reaches its maximum. At the rear of the bubble, the local gradient of the interfacial tension leads to the Marangoni stress, immobilizing the bubble interface. Consequently, a distinct wake structure is formed in the surfactant solution compared to that in pure water. At time T2 when the bubble comes in contact with the free surface, both the bubble and free surface show significant deformations in pure water [see Fig. 3(c)], where the morphology of the free surface is represented by solid black lines. However, the deformations of both bubble and free surface are small in the presence of surfactant. At time T2, surfactants on the bubble interface

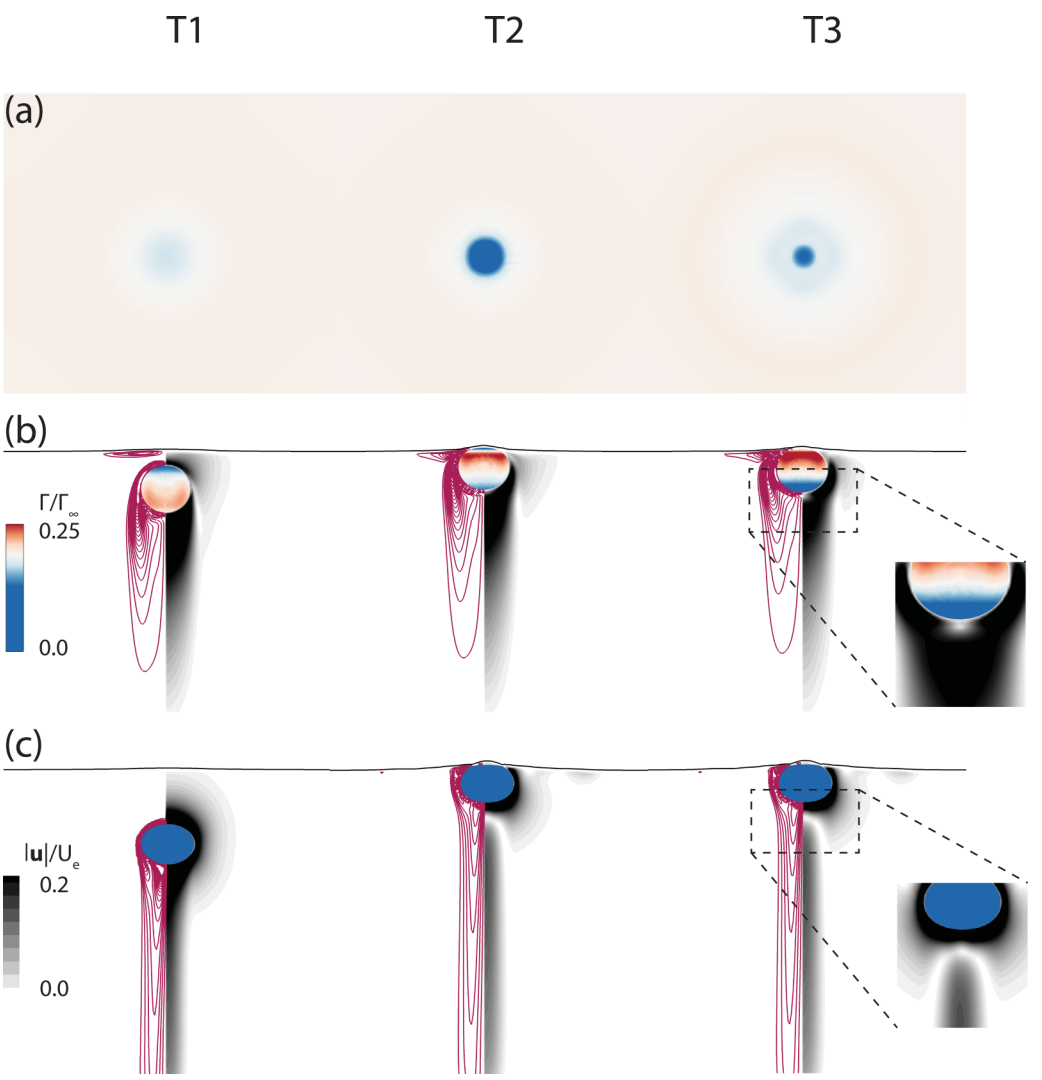

FIG. 3. Color maps show computational results for (a) the interfacial surfactant concentration on the free surface, (b) the velocity magnitude of the flow and the interfacial surfactant concentration on the bubble interface in a 5 mM 1-pentanol solution, and (c) the velocity magnitude of pure water at times T1, T2, and T3. Contours of vorticity magnitude $|\boldsymbol{\Omega}|$ in (b) and (c) are shown at $0.05 : 0.05 : 1.0$. At time T3, the locations of the stagnation points in both pure water and the surfactant solution are visualized in the insets. The bubble radius in both pure water and the surfactant solution is 0.66 mm. The flow velocity in (b) and (c) is normalized by the bubble velocity in the Stokes flow, $U_e = \rho g R^2/(9\mu)$. The flow vorticity in (b) and (c) is normalized by $\Omega_e = U_e/R$.

[Fig. 3(b)] start migrating away from the rear of the bubble, indicating a change in the direction of the interfacial convection on the bubble interface. In the meantime, surfactants on the free surface [Fig. 3(a)] migrate away from the contact region. At time T3, the locations of the stagnation points ($|\mathbf{u}| = 0$ in the wake region) for pure water and the surfactant solution are different. In the surfactant solution, the stagnation point is at the bubble interface, and the bubble has a small coefficient of restitution. However, the stagnation point is farther away from the bubble interface for the pure water, and the bubble exhibits large coefficient of restitution.

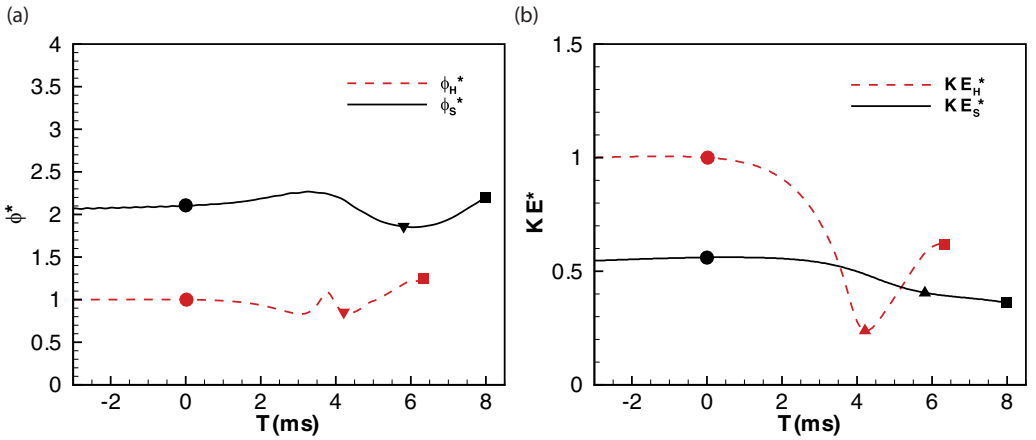

FIG. 4. The evolution of (a) the viscous dissipation rate and (b) kinetic energy are recorded during the collision process in both 0 and 5 mM 1-pentanol solutions, corresponding to subscripts H and S, respectively. Solid circles, triangles, and squares indicate times T1, T2, and T3, respectively.

The small coefficient of restitution in the surfactant solution can be explained by the generation of the vorticity ($\boldsymbol{\Omega} = \nabla \times \mathbf{u}$) during the collision process. In the surfactant solution, the vorticity is generated near the free surface before the bubble approaches the free surface [see Fig. 3(b)]. As the bubble rises towards the free surface, the associated fluid flow creates a nonuniform spatial distribution of the interfacial surfactant concentration along the free surface. The nonuniform distribution of surfactant molecules creates Marangoni stresses, leading to the generation of additional vorticity near the free surface [Fig. 3(b)], which is absent in the pure water [Fig. 3(c)]. The vortical structure near the free surface persists during the entire collision process (see Fig. 3). Following the work of Stone [30], who expressed the viscous energy dissipation rate in terms of vorticity field, we have $\frac{2}{\pi \mathrm{Re}} \int_V \phi dV = \frac{2}{\pi \mathrm{Re}} \int_V \boldsymbol{\Omega}^2 dV + \frac{4}{\pi \mathrm{Re}} \int_S \kappa U_s^2 dS$, where ϕ is the viscous energy dissipation rate and V and S represent the fluid domain and bubble surface, respectively. Therefore, the occurrence of additional vorticity near the free surface in the surfactant solution enhances the viscous dissipation rate and leads to a reduced coefficient of restitution.

Here we quantify the temporal evolution of the viscous dissipation rate ($\phi = \int 2\mu \boldsymbol{E} : \boldsymbol{E} dV$) and kinetic energy ($E_K = \int \frac{1}{2} \rho \boldsymbol{u}^2 dV$) from our computational results, where $\boldsymbol{E}$ is the strain rate tensor. In Fig. 4(a), the normalized viscous dissipation rate is defined as $\phi^* = \phi / \phi_H^{\mathrm{T1}}$, where ϕ_H^{T1} is the viscous dissipation rate in pure water at time T1. The viscous dissipation rate in pure water decreases in the beginning of the collision process. On the other hand, the viscous dissipation rate in the surfactant solution increases. Although the bubble's velocity decreases in the presence of a surfactant, the additional vortical structure induced by the Marangoni stress at the free surface [see Fig. 3(b)] enhances the overall viscous dissipation rate. The kinetic energy in the entire domain is shown in Fig. 4(b), where $E_K^* = E_K / E_{K,H}^{\mathrm{T1}}$ is the normalized kinetic energy. The kinetic energy in pure water increases after collision, which is associated with the bubble's bouncing motion. On the other hand, the kinetic energy in the surfactant solution monotonically decreases during the collision process. To sum up, the enhanced viscous dissipation rate during the collision process in the surfactant solution compared to that in pure water leads to a reduction of the coefficient of restitution.

B. Effect of surfactant concentration

Depending on surfactant concentration, the bubble's collisions exhibit elastic, partially inelastic, and perfectly inelastic behaviors. We first categorize the collision process using a phase diagram. Next, we examine the effect of surfactant concentration on the drag acting on the bubble and the

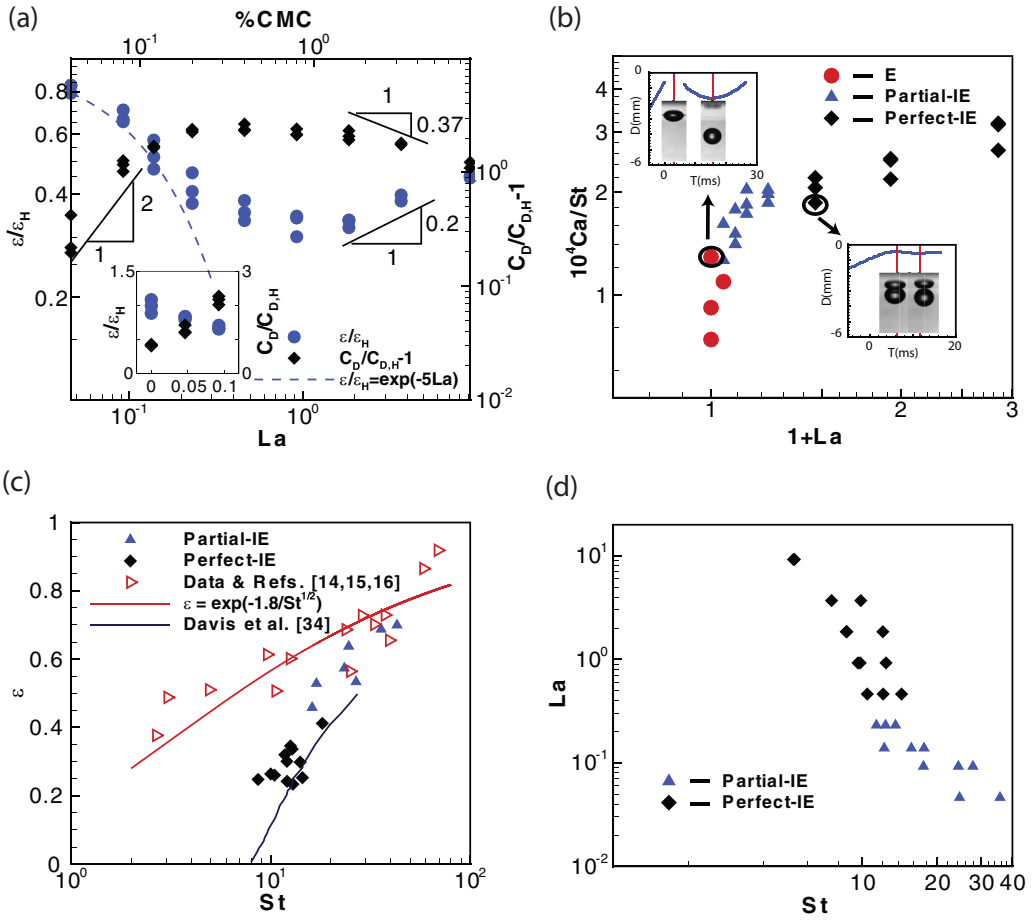

FIG. 5. (a) Normalized coefficient of restitution and drag coefficient are plotted as a function of La number. (b) The phase diagram depicts bubble behavior ranging from elastic (E) to inelastic (Partial-IE) to perfectly inelastic (Perfect-IE) collision, shown in terms of La and Ca/St. (c) The coefficient of restitution is plotted as a function of the St number. (d) The effect of surfactant concentration (La) on the bubble's St number.

coefficient of restitution. In addition, the dynamics of the collision process in the surfactant solution is compared with rigid particles colliding on a rigid wall.

In pure water, the bubble's collision behavior on a free surface is dominated by the viscous drainage process [14–17], and our results follow $\varepsilon_H = \exp(-17\sqrt{\mathrm{Ca/St}})$ (see Appendix C), where $\mathrm{Ca} = U_t\mu/\sigma$ and $\mathrm{St} = 2\rho C_M R U_t/(9\mu)$ [29]. The Capillary number Ca represents the ratio of the viscous force to the surface tension, and the Stokes number St characterizes the relative effect of the inertial force associated with the bubble's added mass to the viscous drag. For surfactant solutions, both mean interfacial surfactant concentration and surface tension solely depend on the Langmuir number La at the equilibrium state. The Langmuir number, $\mathrm{La} = \frac{k_a C_\infty}{k_d \Gamma_\infty}$, is defined as the ratio between the surfactant adsorption and desorption rates happening on the gas-liquid interfaces. For a given β, $\Gamma_o/\Gamma_\infty = 1/(1+\mathrm{La}^{-1})$, and $\sigma/\sigma_0 = 1-\beta\ln(1+\mathrm{La})$, where γ_o is the equilibrium surface concentration when there is no mass transfer between the bulk and surface. Therefore, a large La results in a high interfacial surfactant concentration, reducing the surface tension force and modifying the Marangoni stress. In this work, we use La to characterize the extent of Marangoni stress. In Fig. 5(b), we quantify the coefficient of restitution in terms of La and Ca/St, where La and Ca/St characterize the extent of Marangoni stress and viscous drainage, respectively. When there are

strong Marangoni and viscous effects (La $>$ 0.5 and Ca/St $>$ 2×10^{-4}), bubbles remain attached to the free surface, exhibiting perfectly inelastic collisions. The collisions are elastic when La $\sim$ 0 and Ca/St $<$ 1×10^{-4}.

The drag acting on the bubble prior to the collision is influenced by the surfactant concentration. The drag coefficient is defined as $C_D = 2F/(\rho U_t^2 \pi R^2)$, where F is the drag acting on the bubble. The modified drag due to surfactants can be written as $C_D/C_{D,H}$, where $C_{D,H}$ is the drag acting on a bubble in pure liquids, $C_{D,H} = 48[G(\chi)/\mathrm{Re}][1 + H(\chi)/\mathrm{Re}^{1/2}]$, and coefficients G and H are given in the article by Moore [31]. Surfactants enhance the drag compared to pure water [$C_D/C_{D,H} - 1 > 0$; see Fig. 5(a)]. The extent of drag enhancement depends on the value of La: $C_D/C_{D,H}$ increases at low La and decreases at large La. At small La, the enhanced drag is scaled as $C_D/C_{D,H} - 1 \propto \mathrm{La}^2$, which is consistent with the theory in the Stokes regime [32]. At large La ($1 < \mathrm{La} < 10$), we find it to scale as $C_D/C_{D,H} - 1 \propto \mathrm{La}^{-0.37}$, and a similar trend was found in the numerical study of Wang *et al.* [5] at zero Reynolds number.

A normalized coefficient of restitution can be defined as $\varepsilon/\varepsilon_H$ to eliminate the contribution from the viscous drainage. From Fig. 5(a), surfactants reduce the coefficient of restitution ($\varepsilon/\varepsilon_H < 1$). The effect of a surfactant on $\varepsilon/\varepsilon_H$ is nonmonotonic [Fig. 5(a)], and its maximum reduction occurs at La $\sim$ 1. In the limit of small La, $\varepsilon/\varepsilon_H \sim \exp(-5\,\mathrm{La})$; at large La, $\varepsilon/\varepsilon_H$ increases with La as $\varepsilon/\varepsilon_H \propto \mathrm{La}^{0.2}$.

For both the bubble's drag and its coefficient of restitution, the maximum effect of the surfactant happens when La $\sim O(1)$, which can be explained by the following scaling analysis. The magnitude of Marangoni stress is estimated as $|\nabla\sigma|$ [5]. During the equilibrium state, $\dot{S}_\Gamma = 0$ in Eq. (6), and we get

$$\nabla\sigma = \frac{\sigma_0\beta}{\Gamma/\Gamma_\infty - 1}\frac{\mathrm{La}}{[(1+\mathrm{La})(C/C_\infty)]^2}\nabla\left(\frac{C}{C_\infty}\right). \tag{11}$$

From Eqs. (5) and (7), a balance between the convection and mass source terms provides $|\nabla C| \sim \frac{\Gamma_o U_t}{D_C R}$, where $\Gamma_o = \frac{\mathrm{La}}{1+\mathrm{La}}\Gamma_\infty$. The Marangoni stress normalized by the viscous stress is estimated as $|\nabla_S\sigma|/(\mu U_t/a) \sim \frac{\sigma_0\beta k_a}{D_C\mu k_d}\frac{\mathrm{La}}{(1+\mathrm{La})^2}$. Therefore, the scaling analysis suggests that surfactants have a larger contribution to the collision process compared to the viscous drainage when La $= 1$.

In Fig. 5(c), our experimental data are compared to previously reported experimental data in pure liquids [14–16] as well as the limit of solid particles colliding on a rigid wall [33,34]. At a large Stokes number [St $\sim O(100)$] where there is a low surfactant concentration [low La; see Fig. 5(d)],

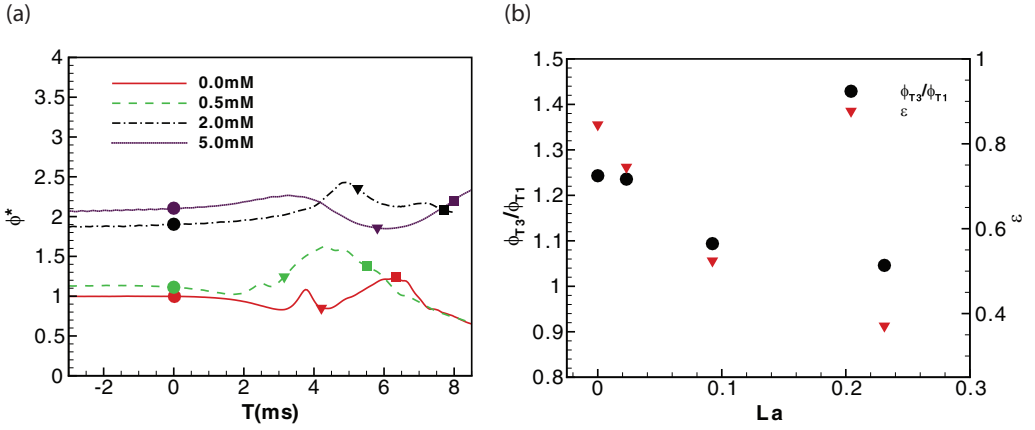

FIG. 6. (a) The evolution of the viscous dissipation rate is recorded during the collision process for different concentrations of 1-pentanol solutions, where solid circles, triangles, and squares indicate times T1, T2, and T3, respectively. (b) The ratio of the viscous dissipation rate between times T3 and T1 and the coefficient of restitution are plotted as a function of the La number. For both (a) and (b), bubble radius is $R = 0.66$ mm.

the bubble's collision behavior is close to the clean one. This clean limit can be characterized by $\varepsilon = \exp(-1.8\,\mathrm{St}^{-1/2})$, which shows a similar scaling as the collision on a rigid wall [29]. However, the coefficient of restitution deviates from this clean limit as St decreases. When $\mathrm{St} < 10$, the surfactant immobilizes both the bubble interface and free surface, and our data resemble a rigid particle colliding into a rigid wall; this behavior can be well predicted by the elastohydrodynamics theory [34]. The collision behavior between these two limits is governed by the Marangoni stresses, and the Langmuir number can be used to describe the coefficient of restitution.

Finally, we quantify the temporal evolution of the viscous dissipation rate in the entire computational domain for different concentrations of the 1-pentanol solution from our numerical results [see Fig. 6(a)]. The ratio of the viscous dissipation rate between times T3 and T1 as a function of Langmuir number in Fig. 6(b) follows a trend similar to that of the coefficient of restitution.

V. CONCLUSION

Collisions between bubbles and a free surface are frequently observed in aquatic environments, and surfactants effectively modify relevant dynamics compared with that in pure water. In this study, we examine the Marangoni effect in the context of a dynamic interfacial problem through both experiments and numerical simulations. In surfactant solutions, we find that the Marangoni stress induces additional vorticity near the free surface, causing extra dissipation and, consequently, reducing the rebound velocity. The Marangoni effect, characterized by the Langmuir number, enhances the bubble's drag and reduces the coefficient of restitution. Their dependence on the surfactant concentration is nonmonotonic. The maximum enhancement of the drag and reduction of the coefficient of restitution occur at $\mathrm{La} \sim O(1)$.

ACKNOWLEDGMENTS

We thank J. W. M. Bush for fruitful discussions. This work was partially supported by a grant from National Science Foundation (CBET-1604423).

APPENDIX A: SURFACE TENSION MEASUREMENTS FOR A 1-PENTANOL SOLUTION

Surface tension for an aqueous solution of 1-pentanol at 21°C is measured as a function of concentration. Figure 7 compares our measured data to the empirical relationship provided in the

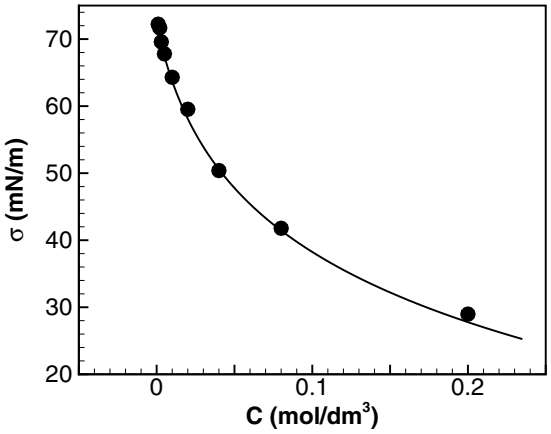

FIG. 7. Measured surface tensions for the 1-pentanol solution (black solid circles); the solid line is the Szyszkowski equation [21].

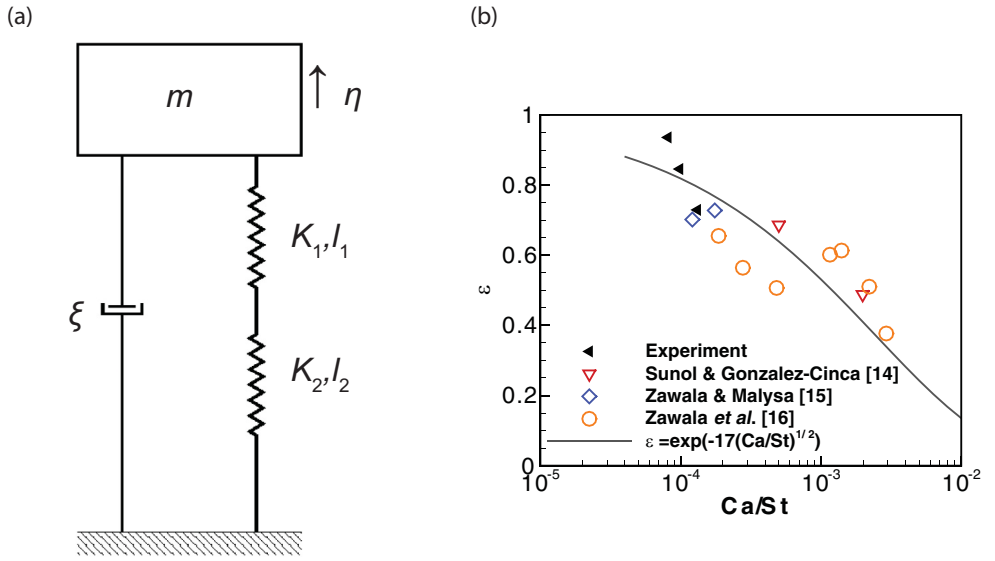

FIG. 8. (a) Mass-spring-damper model: two springs are connected in series; the dashpot and springs are connected in parallel. K_1 and K_2 are the spring stiffness of the free surface and bubble, respectively; the natural length l_1 corresponds to an undeformed free surface, while l_2 incorporates the initial deformation of the rising bubble; m is the added mass of the bubble; ξ is the damping ratio, which incorporates the contribution to the drag from both the viscous force and Marangoni stress. (b) The derived relationship between the coefficient of restitution ε and Ca/St is provided based on data from our experiments and the literature.

literature [21]. This empirical relationship is described by the Szyszkowski equation,

$$\sigma = \sigma_0 - \frac{\mathscr{R}T}{\omega}\ln(1 + kC), \tag{A1}$$

where $\omega = 1.48 \times 10^5$ m^2/mol and $k = 66$ dm^3/mol [21].

APPENDIX B: UNCERTAINTY QUANTIFICATION FOR EXPERIMENTS

There are two major uncertainty sources in the experimental postprocessing procedure. They are the uncertainties of the calibration process, and the variation in the preselected threshold for bubble image binarization. After each uncertainty is calculated, the total uncertainty is synthesized by the Taylor series approximation of the elemental uncertainties. The uncertainty of the calibration process is straightforward, and here we report the methodology for uncertainty due to a preselected threshold.

The variation of the threshold during image binarization affects the detected bubble profile and shape, which leads to uncertainty in the estimation of the bubble's center, radius, deformation, surface area, volume, and other derived quantities. This uncertainty is quantified by examining the root mean square of the reported parameters by continuously changing the threshold values.

APPENDIX C: UNDERDAMPED MASS-SPRING SYSTEM

The dynamics of the bubble's collision process are modeled as an underdamped mass-spring system [see Fig. 8(a)],

$$m\frac{d^2\eta}{dt} + \mathscr{C}_{\mu,C}\frac{d\eta}{dt} + \mathscr{C}_\sigma\eta = 0, \tag{C1}$$

where $m = \frac{4}{3}\pi R^3 \rho C_M$ is the added mass of the bubble, $\mathscr{C}_{\mu,C}$ characterizes the drag during the collision process in a surfactant solution, and $\mathscr{C}_\sigma = K_1 K_2/(K_1 + K_2) = k_1 k_2 \sigma/(k_1 + k_2) = \mathscr{K}\sigma$, where $K_i (i = 1,2) = \sigma k_i$. Rewriting Eq. (C1) gives

$$\frac{d^2\eta}{dt} + 2\xi(\mathrm{St},\mathrm{Ca},\mathrm{La})\omega\frac{d\eta}{dt} + \omega^2\eta = 0, \tag{C2}$$

where $\xi = \mathscr{C}_{\mu,C}/(2m\omega)$ is the damping ratio and $\omega = \sqrt{\mathscr{K}\sigma/m}$ is the natural frequency. A reduced bouncing velocity occurs due to the viscous drag (low St) and Marangoni stress (large La). During the collision process, the normalized bubble velocity is expressed as

$$U/U_t = \dot{\eta}(t)/U_t = e^{-\xi\omega t}\cos(\omega t\sqrt{1-\xi^2}). \tag{C3}$$

In our experiments, the damping ratio ξ and natural frequency ω are calculated using these relationships $\varepsilon = -U_{\mathrm{T3}}/U_{\mathrm{T1}} = e^{-\xi\pi/\sqrt{1-\xi^2}}$ and $\omega = \pi(1-\xi^2)^{-1/2}/(\mathrm{T3} - \mathrm{T1})$, respectively.

In a pure fluid, $\mathscr{C}_{\mu,C} = \mathscr{C}_\mu = a\mu R$ [29], where a is a constant. Therefore, the damping ratio can be written as $\xi = \frac{a}{\sqrt{24\pi\mathscr{K}}}\sqrt{\frac{\mathrm{Ca}}{\mathrm{St}}}$. Since $\frac{\mathrm{Ca}}{\mathrm{St}} \sim O(10^{-4})$, $\varepsilon \sim e^{-\mathscr{M}\sqrt{\frac{\mathrm{Ca}}{\mathrm{St}}}}$ in the case of $\xi \ll 1$, where $\mathscr{M}$ is a fitting parameter. By combining data from our experiments and literature [14–16], we find that $\mathscr{M} = 17$ provides the best fit [see Fig. 8(b)].

[1] R. B. Fdhila and P. C. Duineveld, The effect of surfactant on the rise of a spherical bubble at high Reynolds and Peclet numbers, Phys. Fluids **8**, 310 (1996).

[2] S. Takagi and Y. Matsumoto, Surfactant effects on bubble motion and bubbly flows, Annu. Rev. Fluid Mech. **43**, 615 (2011).

[3] A. Frumkin and V. G. Levich, On surfactants and interfacial motion, Zh. Fiz. Khim. **21**, 1183 (1947) (in Russian).

[4] B. Cuenot, J. Magnaudet, and B. Spennato, The effects of slightly soluble surfactants on the flow around a spherical bubble, J. Fluid Mech. **339**, 25 (1997).

[5] Y. Wang, D. T. Papageorgiou, and C. Maldarelli, Increased mobility of a surfactant-retarded bubble at high bulk concentrations, J. Fluid Mech. **390**, 251 (1999).

[6] M. Fukuta, S. Takagi, and Y. Matsumoto, Numerical study on the shear-induced lift force acting on a spherical bubble in aqueous surfactant solutions, Phys. Fluids **20**, 040704 (2008).

[7] Y. Zhang and J. A. Finch, A note on single bubble motion in surfactant solutions, J. Fluid Mech. **429**, 63 (2001).

[8] Y. Tagawa, S. Takagi, and Y. Matsumoto, Surfactant effect on path instability of a rising bubble, J. Fluid Mech. **738**, 124 (2014).

[9] M. Muradoglu and G. Tryggvason, A front-tracking method for computation of interfacial flows with soluble surfactants, J. Comput. Phys. **227**, 2238 (2008).

[10] S. Tasoglu, U. Demirci, and M. Muradoglu, The effect of soluble surfactant on the transient motion of a buoyancy-driven bubble, Phys. Fluids **20**, 040805 (2008).

[11] M. Muradoglu and G. Tryggvason, Simulations of soluble surfactants in 3D multiphase flow, J. Comput. Phys. **274**, 737 (2014).

[12] L. Doubliez, The drainage and rupture of a non-foaming liquid film formed upon bubble impact with a free surface, Int. J. Multiphase Flow **17**, 783 (1991).

[13] H. K. Tsao and D. L. Koch, Observations of high Reynolds number bubbles interacting with a rigid wall, Phys. Fluids **9**, 44 (1997).

[14] F. Suñol and R. González-Cinca, Rise, bouncing and coalescence of bubbles impacting at a free surface, Colloids Surf. A **365**, 36 (2010).

[15] J. Zawala and K. Malysa, Influence of the impact velocity and size of the film formed on bubble coalescence time at water surface, Langmuir **27**, 2250 (2011).
[16] J. Zawala, S. Dorbolo, D. Terwagne, N. Vandewalle, and K. Malysa, Bouncing bubble on a liquid/gas interface resting or vibrating, Soft Matter **7**, 6719 (2011).
[17] R. Manica, E. Klaseboer, and D. Y. C. Chan, The impact and bounce of air bubbles at a flat fluid interface, Soft Matter **12**, 3271 (2016).
[18] T. S. Light, S. Licht, A. C. Bevilacqua, and K. R. Morash, The fundamental conductivity and resistivity of water, Electrochem. Solid-State Lett. **8**, E16 (2005).
[19] S. Takagi, T. Uda, Y. Watanabe, and Y. Matsumoto, Behavior of a rising bubble in water with surfactant dissolution (1st report, steady behavior), Trans. Jpn. Soc. Mech. Eng. B **69**, 2192 (2003).
[20] V. B. Fainerman and S. V. Lylyk, Dynamic surface-tension and kinetics of adsorption in solutions of normal alcohols, Colloid J. **44**, 538 (1982).
[21] M. J. Hey and P. G. Kippax, Surface tensions of mixed aqueous solutions of tert-butanol and n-pentanol, Colloids Surf. A **262**, 198 (2005).
[22] S. Dabiri, A. Doostmohammadi, M. Bayareh, and A. M. Ardekani, Rising motion of a swarm of drops in a linearly stratified fluid, Int. J. Multiphase Flow **69**, 8 (2015).
[23] S. Dabiri and G. Tryggvason, Heat transfer in turbulent bubbly flow in vertical channels, Chem. Eng. Sci. **122**, 106 (2015).
[24] B. P. Leonard, A stable and accurate convective modeling procedure based on quadratic upstream interpolation, Comput. Methods Appl. Mech. Eng. **19**, 59 (1979).
[25] R. Borges, M. Carmona, B. Costa, and W. S. Don, An improved weighted essentially non-oscillatory scheme for hyperbolic conservation laws, J. Comput. Phys. **227**, 3191 (2008).
[26] R. D. Falgout and U. M. Yang, HYPRE: A library of high performance preconditioners, in *Computational Science—ICCS 2002*, Lecture Notes in Computer Science Vol. 2331 (Springer, Berlin, 2002), p. 632.
[27] See Supplemental Material at http://link.aps.org/supplemental/10.1103/PhysRevFluids.2.043601 for two movies. Moive 1 shows the temporal evolution of both the vertical position of the bubble center and the bubble's translational velocity in both pure water and the 5 mM 1-pentanol solution. The bubble's collision process in the 5 mM 1-pentanol solution via numerical simulation is shown in Movie 2.
[28] H. Lamb, *Hydrodynamics* (Cambridge University Press, Cambridge, 1932).
[29] R. Zenit and D. Legendre, The coefficient of restitution for air bubbles colliding against solid walls in viscous liquids, Phys. Fluids **21**, 083306 (2009).
[30] H. A. Stone, An interpretation of the translation of drops and bubbles at high Reynolds numbers in terms of the vorticity field, Phys. Fluids **5**, 2567 (1993).
[31] D. W. Moore, The velocity of rise of distorted gas bubbles in a liquid of small viscosity, J. Fluid Mech. **23**, 749 (1965).
[32] L. G. Leal, *Advanced Transport Phenomena: Fluid Mechanics and Convective Transport Processes* (Cambridge University Press, Cambridge, 2007).
[33] G. G. Joseph, R. Zenit, M. L. Hunt, and A. M. Rosenwinkel, Particle-wall collisions in a viscous fluid, J. Fluid Mech. **433**, 329 (2001).
[34] R. H. Davis, J. M. Serayssol, and E. J. Hinch, The elastohydrodynamic collision of two spheres, J. Fluid Mech. **163**, 479 (1986).